MITOR: Jurnal Teknik Elektro

Grid Tie Inverter Connected to a Three-Phase Power Grid Using Photovoltaic

Setiyono*
Jurusan Teknik Elektro Fakultas Teknologi Industri – Universitas Gunadarma
Jakarta, Indonesia
*setiyono@staff.gunadarma.ac.id

Abstract – *Indonesia is a country that is crossed by the equator and has abundant sources of solar energy, so it has great potential for building solar power plants. So far, national power plants have been supported by coal and oil energy sources, so this will have an impact on global warming/, increased carbon emissions in the air/, damage to nature and losses in terms of development costs. To reduce losses in conventional power plants, an effective solution is needed/, one of which is utilizing solar energy. This research describes a photovoltaic electricity generator connected to a stand-alone electricity network or better known as a Grid Tie Inverter (GTI). The aim is to supply additional power to a three-phase grid system when the load continues to increase. This GTI consists of several main parts/, namely the SunPower SPR-315E-WHT-D 200Wp PV/, Boost Converter circuit/, three-arm three-phase inverter transistor unit/, filter circuit/, and PWM signal generator control system. The method used in this research is to build a GTI simulation model for a three-wire power system using Matlab Simulink. The simulation results show that the output voltage shape of the three-wire GTI is close to a sinusoid with a Total Harmonic Distortion (THD) content of 2.47%/, with a power that can be added to the electricity network of 250 W.*

Keywords – *Photovoltaic System; Grid Tie Inverter; Boost Converter; Three-Phase Inverter; Total Harmonic Distortion.*

I. Introduction

THE development of renewable energy continues to be pursued to enhance national energy security. One of the pollution-free energy sources being promoted is solar energy, which is converted into electrical energy. The installed capacity of renewable energy power plants has grown significantly, with solar power plants (PLTS) increasing from 0.3 GW in 2022 to 5 GW in the Hymne scenario and 26 GW in the Mars scenario by 2033 [1]. These solar power plants are targeted to replace coal and oil-fired power plants, which have been the primary energy sources for conventional power generation [2].

A Grid Tie Inverter (GTI) is a power generation system connected to the main electrical grid [3]. It is primarily used to convert direct current (DC) energy from solar panels into alternating current (AC) energy [4]. Typically, GTIs are rooftop solar power systems installed on residential homes. This option is preferred in Indonesia due to the country's equatorial location, which provides abundant solar radiation [5]. The main components of a GTI system include:

1. DC Input: The power source generated by the solar panel.
2. Maximum Power Point Tracking (MPPT): Optimizes power output by continuously monitoring and adjusting voltage and current levels.
3. Inverter: Converts DC voltage into AC electricity using electronic devices and control systems.
4. Grid Synchronizer: Detects and matches phase and frequency between the GTI and the grid.
5. Monitoring and Control System: Tracks and adjusts the performance of solar panels in generating electricity.

To connect a GTI to the grid, several requirements must be met, including voltage level, phase count, phase sequence, and output frequency [6]. A GTI can help reduce electricity bills when operating during the daytime [7].

A solar panel is a device used to convert sunlight into electrical energy. It is expected to provide optimal power output under various conditions, whether receiving maximum or minimal solar irradiation. This opti-

The manuscript was received on December 7, 2024, revised on March 20, 2025, and published online on March 28, 2025. Emitor is a Journal of Electrical Engineering at Universitas Muhammadiyah Surakarta with ISSN (Print) 1411 – 8890 and ISSN (Online) 2541 – 4518, holding Sinta 3 accreditation. It is accessible at https://journals2.ums.ac.id/index.php/emitor/index.

mization process is managed through Maximum Power Point Tracking (MPPT) techniques [8, 9]. The MPPT algorithm searches for the maximum power point by adjusting voltage levels using a DC-DC converter [10, 11]. However, conventional MPPT algorithms experience power oscillations during steady-state conditions and potential power losses in the system. Conventional maximum power point tracking (MPPT) algorithms for photovoltaic systems, particularly the perturbation and observation (P&O) method, often experience power oscillations during steady-state conditions and potential power losses [12, 13]. These oscillations can lead to inefficiencies in grid connections and reduced output power [13, 14]. To address these issues, researchers have proposed various modifications to MPPT algorithms. These include self-adaptable step sizes [12], median filtering algorithms [13], and hybrid approaches combining genetic algorithms with P&O [15]. Other improvements focus on dynamic boundary conditions [16], variable PWM step-sizes [17], and irradiance change identifiers [18]. These modified algorithms aim to reduce steady-state oscillations, improve tracking efficiency, and enhance performance under various atmospheric conditions, including partial shading [15, 19]. To minimize these losses, the Modified Incremental Conductance Algorithm has been introduced, which reduces oscillations and incorporates variable step size to accelerate tracking of the maximum power point [20].

Moreover, the power output from solar panels is affected by their positioning and orientation in receiving sunlight [21, 22]. There are three primary configurations of solar power systems:

1. On-Grid PLTS: Connected directly to the electrical grid.
2. Off-Grid PLTS (Stand-Alone): Independent of the electrical grid, typically using battery storage.
3. Hybrid PLTS: A combination of solar power with other types of power generation [23].

Several previous studies have explored GTI applications. Reinard developed a Grid Tie Inverter with Limiter (GTIL) to prevent excess energy from flowing back into the grid. When solar panel production exceeds the connected load, GTIL restricts energy output to match the load capacity [24]. Setyo Purnomo designed a micro-inverter that demonstrated better performance than string inverters under varying weather conditions, showing significant differences between the two systems [25]. Retno analyzed the operation of PLTS On-Grid inverters, concluding that they perform efficiently when the minimum voltage range is maintained between 400V{800V in Indonesia's three-phase 220V/380V grid [26].

This study aims to develop a three-phase grid tie inverter model using a photovoltaic system with DC-DC converter control and a three-leg IGBT inverter. The objective is to optimize energy conversion efficiency and enhance system reliability under different operational conditions.

II. Research Methods

The method used in this research involves designing a grid tie inverter system with photovoltaic (PV) panels as a DC voltage source, which is electrically injected into a three-phase grid. The system design is then modeled using MATLAB Simulink simulation tools. The overall system design can be seen in Figure 1.

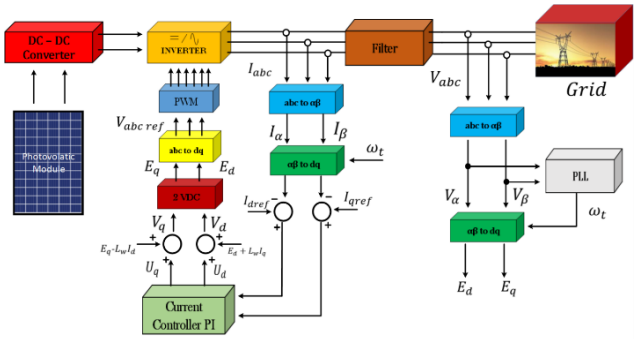

Figure 1: Design of a grid tie inverter system based on solar power generation.

Figure 1 illustrates the workflow of the system block as a whole. The first component is the photovoltaic panel, which functions to convert solar energy into electricity. The DC-DC converter is responsible for increasing the DC voltage from the PV panel. The inverter plays a crucial role in converting DC voltage into three-phase AC voltage. The filter is used to eliminate ripples or harmonics in the three-phase output voltage of the inverter, ensuring a smoother sinusoidal voltage waveform. Meanwhile, the grid represents the main power generation system from the national electric company (PLN).

The core function of this system lies in the operation of the inverter, which requires precise switching pulses. These pulses demand mathematical analysis, which will be discussed further in the analysis and discussion section. Once the system block is established, the next step involves designing the electronic system to determine the appropriate component values.

Figure 2a illustrates the electrical design of the grid tie inverter system, whereas Figure 2b presents the modeled GTI system using MATLAB Simulink.

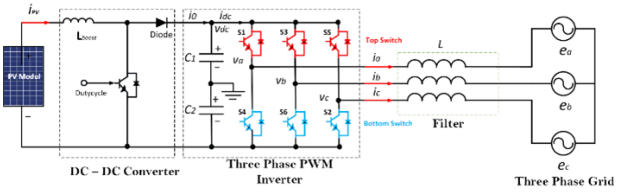

(a) `Grid Tie Inverter` circuit diagram.

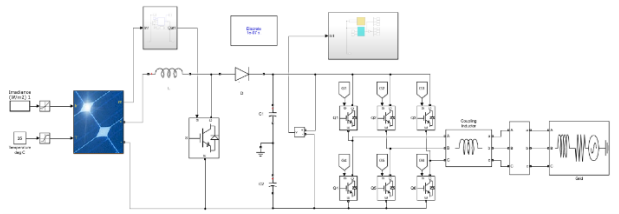

(b) `Grid Tie Inverter` model in `MATLAB Simulink`.

Figure 2: `Grid Tie Inverter` electrical design and simulation model.

i. Technical Data of Photovoltaic System

The photovoltaic system used in this study is characterized by several parameters, as shown in Table 1 and Table 2.

Table 1: Technical Data of the `Photovoltaic` System.

`Module Data`	`Model Parameters`
Module Type	SunPower SPR-315E-WHT-D
Light generated current I_L	6.1461 A
Open Circuit Voltage	64.6 V
Diode saturation current (I_o)	6.5043e-12 A
Voltage at MPP	54.7 V
Diode ideality factor	0.9507 A
Temperature coefficient of V_o	-0.2726 %/°C
Shunt Resistance R_{sh}	430.0559 Ω
Cells per module	96
Series Resistance R_s	0.43042 Ω
Short circuit current I_{sc}	6.14 A
Current at MPP	5.76 A
Temperature coefficient of I_{sc}	0.061694%/°C
Number of series strings	5
Number of parallel strings	64

III. Results and Discussion

i. Analysis of the DC-DC Converter Section

The photovoltaic panel used in this study is the `SunPower SPR-315E-WHT-D` type, with its technical parameters provided in Table 1. The PV module consists of 5 series-connected strings and 64 parallel-connected strings. The power-voltage (`P{V}`) characteristics of this photovoltaic module can be analyzed in Figure 3.

From the graph in Figure 3, the maximum short-circuit current is observed to be 6.14 A, and the maximum open-circuit voltage reaches 65 V. At an irradiance level of 1 kW/m^2, the generated power is approximately 300 W.

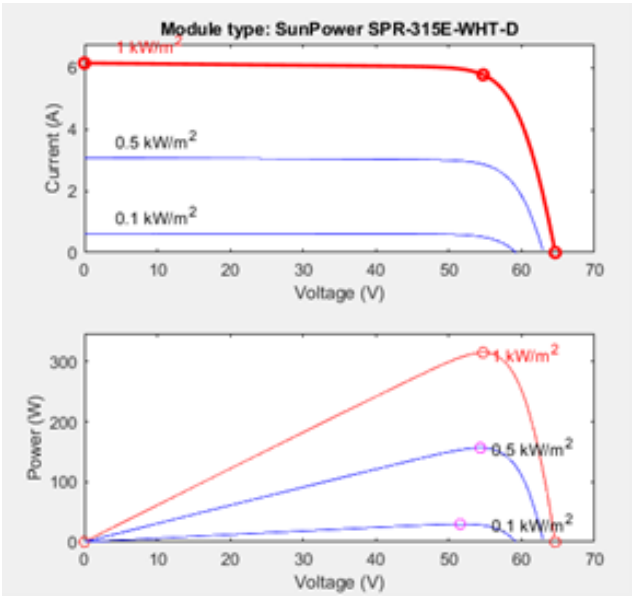

Figure 3: P–V Characteristics of the SunPower SPR-315E-WHT-D PV Module.

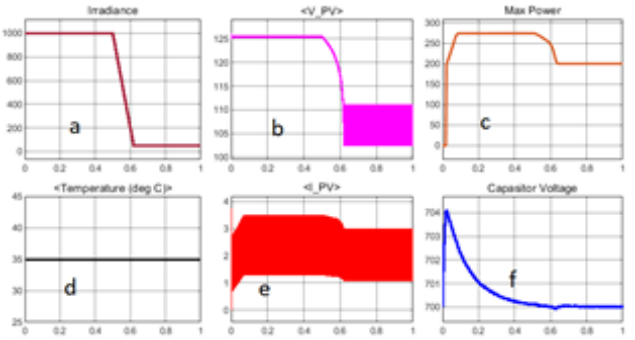

Figure 4: Electrical Parameters of the PV and DC-Link Capacitor Voltage.

Figure 4 illustrates various electrical parameters of the PV and DC-link capacitor voltage:

1. Figure 4a shows the solar irradiance level, which is set to 1000 W/m^2.
2. Figure 4b represents the output voltage of the photovoltaic panel, which is measured at 125 V.
3. Figure 4c displays the maximum power output of the PV panel at a temperature of 35°C and an irradiance of 1000 W/m^2, calculated as:

$$P_m = V_{pv} \times I_{pv} = 125 \times 2 = 250 \text{ W} \quad (1)$$

4. Figure 4d indicates the ambient temperature, which is set at 35°C.
5. Figure 4e shows the average current output from the photovoltaic panel, which is approximately 2 A.
6. Figure 4f presents the voltage at the DC-link capacitor of the inverter, which reaches 700 V.

Table 2: Technical Parameters of the `Grid Tie Inverter` System.

DC-DC Converter		Inverter and Grid	
Inductance L	4 mH	Switches $T_1, T_2, T_3, T_4, T_5, T_6$	IGBT internal resistance 0.001 Ω
Switch S	IGBT internal resistance 0.001 Ω	Coupling Inductor	0.283 mH
Diode	$R_{on} = 0.001$ Ω, Forward voltage = 0.8 V	Grid Voltage V_{L-L}	400 V, 50 Hz, Y-connected
Capacitor C_1 and C_2	4700 μF, 350 V	Load	$R = 1$ Ω, $L = 0.001$ H
V_{DC}	700 V		
V_{PV}	125 V		
V_{grid}	400 V_{L-L}		

ii. Analysis of Boost Converter

The boost converter trigger pulse is used to activate the IGBT switch in Figure 2a, controlling the duty cycle. Various designs use Pulse Width Modulation (PWM)-based control to regulate the switch's ON/OFF state, integrating it with an MPPT algorithm. The MPPT algorithm is essential for adjusting the PWM duty cycle width, ensuring that the PV system operates at its maximum power point, even under varying light intensity and temperature conditions.

The fundamental principle of MPPT using PWM duty cycle control is to convert DC power from the PV system by increasing its voltage to the boost converter output voltage. The PWM trigger pulse in this DC-DC converter is generated by adjusting the duty cycle, which is the ratio of ON time to OFF time. Duty cycle control directly influences the output voltage of the boost converter, which in turn affects the power output of the PV panel. The following is the P-code implementation of the MPPT algorithm 1 using the Perturb and Observe method:

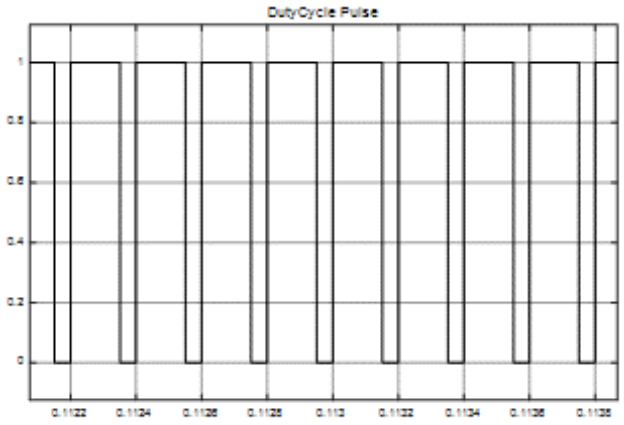

Figure 5: Trigger Pulse Signal for Duty Cycle Control.

Figure 5 represents the trigger pulse signal with duty cycle control for IGBT switch activation in the boost converter circuit. The waveform exhibits a 1V amplitude with a switching frequency of 5 kHz.

Algorithm 1 MPPT Controller using Perturb & Observe Algorithm

Input: `Param`, `Enabled`, `V`, `I`
Output: `D` (Duty cycle of the boost converter)
`Dinit` ← `Param(1)`
`Dmax` ← `Param(2)`
`Dmin` ← `Param(3)`
`deltaD` ← `Param(4)`
Persistent: `Vold, Pold, Dold`
if `Vold` is empty **then**
    `Vold` ← 0, `Pold` ← 0, `Dold` ← `Dinit`
end if
`P` ← `V` × `I`
`dV` ← `V - Vold`
`dP` ← `P - Pold`
if `dP` ≠ 0 **and** `Enabled` ≠ 0 **then**
    if `dP` < 0 **then**
        if `dV` < 0 **then**
            `D` ← `Dold - deltaD`
        else
            `D` ← `Dold + deltaD`
        end if
    else
        if `dV` < 0 **then**
            `D` ← `Dold + deltaD`
        else
            `D` ← `Dold - deltaD`
        end if
    end if
else
    `D` ← `Dold`
end if
if `D` ≥ `Dmax` **or** `D` ≤ `Dmin` **then**
    `D` ← `Dold`
end if
`Dold` ← `D`, `Vold` ← `V`, `Pold` ← `P`

iii. Analysis of the DC Link Capacitor

The inverter circuit in Figure 2a is equipped with a `DC link capacitor` that functions to filter the DC voltage ripple originating from the `DC-DC converter`. Capacitors C_1 and C_2 are connected in series to divide the DC source voltage, where the neutral point is where voltage fluctuations occur. The DC voltage value, V_{DC}, can be expressed using the following equation [28]: The total capacitance of C_1 and C_2, denoted as C_{tot}, can be determined using Equation (2). In this equation, I_R represents the average current, while E corresponds to the DC side voltage. The frequency is denoted as f, and the voltage fluctuation is represented by $\bar{V}_n$. Additionally, V_n indicates the average voltage. These parameters collectively define the required capacitance to ensure stable voltage levels in the system.

$$C_{tot} = \frac{I_R\sqrt{2}}{2\pi f \frac{2E\bar{V}_n}{V_n}} \tag{2}$$

In the system design, the capacitance values are given as:

$$C_1 = 4700\,\mu F, \quad 350V$$
$$C_2 = 4700\,\mu F, \quad 350V$$

These capacitors play a crucial role in maintaining voltage stability in the inverter circuit, ensuring that the `DC link` provides a steady voltage level before conversion to AC.

iv. Inverter Analysis

The three-phase `inverter` is built using three legs, each consisting of two `IGBT switches`, as shown in Figure 2a. Each leg consists of a pair of switches connected in series, and the three pairs of switches are arranged in parallel. The switches located in the upper position are called `top switches` (`Ts`, S_1, S_3, S_5), while the lower switches are referred to as `bottom switches` (S_2, S_4, S_6). The operation of the switches is controlled using `PWM pulse signals`.

The inverter operates by generating three-phase output voltages denoted as V_{ao}, V_{bo}, and V_{co}. There are eight possible switching states in the inverter circuit, where a logic state of 000 for the top switches represents an `OFF` condition, and the bottom switches follow the opposite logic, 111 (ON state). The inverter converts DC voltage from the photovoltaic system into pure AC voltage, which is then synchronized with the electrical grid. The switching operation of the three-phase inverter is presented in Table 3.

Table 3 presents the inverter output voltages for various switching conditions.

Table 3: Switching States and Output Voltages of the Three-Phase Inverter

S_1 S_4	S_3 S_6	S_5 S_2	V_{ao}	V_{bo}	V_{co}
0	0	0	$-\frac{V_{dc}}{2}$	$-\frac{V_{dc}}{2}$	$-\frac{V_{dc}}{2}$
0	0	1	$-\frac{V_{dc}}{2}$	$-\frac{V_{dc}}{2}$	$+\frac{V_{dc}}{2}$
0	1	0	$-\frac{V_{dc}}{2}$	$+\frac{V_{dc}}{2}$	$-\frac{V_{dc}}{2}$
0	1	1	$-\frac{V_{dc}}{2}$	$+\frac{V_{dc}}{2}$	$+\frac{V_{dc}}{2}$
1	0	0	$+\frac{V_{dc}}{2}$	$-\frac{V_{dc}}{2}$	$-\frac{V_{dc}}{2}$
1	0	1	$+\frac{V_{dc}}{2}$	$-\frac{V_{dc}}{2}$	$+\frac{V_{dc}}{2}$
1	1	0	$+\frac{V_{dc}}{2}$	$+\frac{V_{dc}}{2}$	$-\frac{V_{dc}}{2}$
1	1	1	$+\frac{V_{dc}}{2}$	$+\frac{V_{dc}}{2}$	$+\frac{V_{dc}}{2}$

The output voltages of a three-phase inverter can be mathematically expressed as sinusoidal waveforms that vary with time, as given in Equations (3), (4), and (5) [29]. The phase voltage v_a is represented as a function of the maximum voltage amplitude V_m and the angular frequency ω, as shown in Equation (3).

$$v_a = V_m \sin(\omega t) \tag{3}$$

Similarly, the second-phase voltage v_b exhibits a phase shift of $\frac{2\pi}{3}$ radians behind v_a, as described in Equation (4).

$$v_b = V_m \sin(\omega t - \frac{2\pi}{3}) \tag{4}$$

Likewise, the third-phase voltage v_c leads v_a by $\frac{2\pi}{3}$ radians, as given by Equation (5).

$$v_c = V_m \sin(\omega t + \frac{2\pi}{3}) \tag{5}$$

In these equations, V_m represents the peak amplitude of the voltage, while ω denotes the angular frequency. The three-phase voltages v_a, v_b, and v_c maintain a consistent phase shift of 120°, ensuring a balanced three-phase system. This balanced nature is crucial for efficient power transmission and minimizing harmonic distortions in grid-tied inverter applications. The voltage analysis for each phase of the inverter, denoted as v_i, can be described by the relationship between the load voltage v_L and the grid voltage v_g, as expressed in Equation (6).

$$v_i = v_L + v_g \tag{6}$$

Considering the influence of the inductor in the circuit, the voltage equation can be rewritten to include the inductance L and the time derivative of the current i, leading to Equation (7).

$$v_i = L\frac{di}{dt} + v_g \tag{7}$$

By rearranging Equation (7), the grid voltage v_g can be expressed in terms of the inverter voltage v_i and the inductance effect, as shown in Equation (8).

$$v_g = v_i - L\frac{di}{dt} \tag{8}$$

Here, the grid voltage v_g is assumed to be equal to the phase electromotive forces e_a, e_b, and e_c. These equations are essential for understanding the interaction between the inverter output and the grid, particularly in analyzing voltage regulation and dynamic performance in grid-tied inverter applications.

From Equation (8), the three-phase system voltage in the `abc` reference frame can be expressed in matrix notation, as shown in Equation (9). This representation highlights the relationship between the inverter output voltages and the grid voltages in each phase.

$$\begin{bmatrix} v_{ga} \\ v_{gb} \\ v_{gc} \end{bmatrix} = \begin{bmatrix} v_{ia} - L\frac{di_a}{dt} \\ v_{ib} - L\frac{di_b}{dt} \\ v_{ic} - L\frac{di_c}{dt} \end{bmatrix} \tag{9}$$

To facilitate analysis and control, the transformation from the stationary three-phase (`abc`) reference frame to the two-phase ($\alpha\beta$) reference frame is applied using the Clarke transformation, as defined in Equation (10). This transformation simplifies calculations by converting the three-phase system into an equivalent two-phase representation.

$$\begin{bmatrix} v_{g\alpha} \\ v_{g\beta} \end{bmatrix} = \frac{2}{3}\begin{bmatrix} 1 & -\frac{1}{2} & -\frac{1}{2} \\ 0 & \frac{\sqrt{3}}{2} & -\frac{\sqrt{3}}{2} \end{bmatrix}\begin{bmatrix} v_{ga} \\ v_{gb} \\ v_{gc} \end{bmatrix} \tag{10}$$

By substituting Equation (9) into Equation (10), the transformation can be rewritten as follows:

$$\begin{bmatrix} v_{g\alpha} \\ v_{g\beta} \end{bmatrix} = \frac{2}{3}\begin{bmatrix} 1 & -\frac{1}{2} & -\frac{1}{2} \\ 0 & \frac{\sqrt{3}}{2} & -\frac{\sqrt{3}}{2} \end{bmatrix}\begin{bmatrix} v_{ia} - L\frac{di_a}{dt} \\ v_{ib} - L\frac{di_b}{dt} \\ v_{ic} - L\frac{di_c}{dt} \end{bmatrix} \tag{11}$$

Finally, simplifying the transformation yields Equation (12), where the two-phase ($\alpha\beta$) voltage components are directly related to the inverter output voltages and the inductive effects.

$$\begin{bmatrix} v_{g\alpha} \\ v_{g\beta} \end{bmatrix} = \begin{bmatrix} v_{i\alpha} - L\frac{di_\alpha}{dt} \\ v_{i\beta} - L\frac{di_\beta}{dt} \end{bmatrix} \tag{12}$$

This transformation plays a crucial role in analyzing and controlling grid-tied inverters, as it enables efficient control of active and reactive power flow while simplifying the implementation of advanced control strategies in modern power systems.

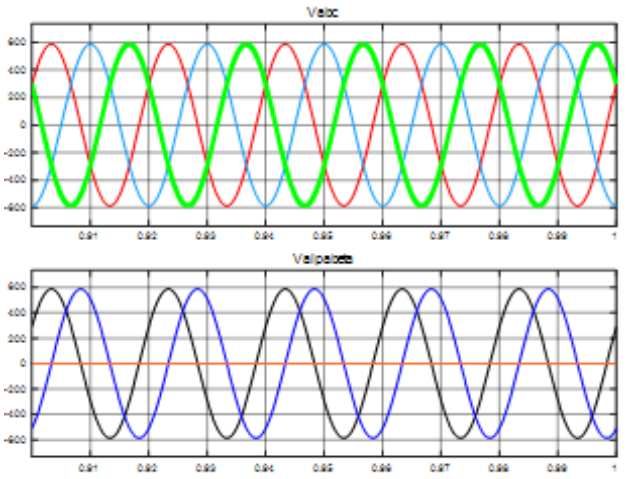

Figure 6: Three-phase balanced waveform and $\alpha\beta$ voltage waveform

v. Transformation from abc to $\alpha\beta$ and dq Frames

Figure 6 represents the transformation from the *abc* coordinate system to the two-axis $\alpha\beta$ coordinate system ($abc \rightarrow \alpha\beta$). The three-phase sinusoidal waveform (*abc*) with a peak-to-peak amplitude of 600 V exhibits a 120° phase difference between each phase. Through the Clarke transformation, this waveform is converted into the $\alpha\beta$ coordinate system, where the output voltage remains at 600 Vpp but now has a 90° phase shift between the α and β components.

This phase shift condition applies to a balanced system. However, in an unbalanced system, numerical calculations and more complex analysis are required to determine the exact phase angle difference between the α and β components. The frequency of both waveforms remains identical at 50 Hz.

The transformation from the $\alpha\beta$ frame to the *dq* frame is essential for analyzing and controlling grid-tied inverters. This transformation is mathematically expressed in Equation (13), which relates the voltage components in the $\alpha\beta$ reference frame to the *dq* reference frame through a rotational transformation matrix.

$$\begin{bmatrix} v_{gd} \\ v_{gq} \end{bmatrix} = \begin{bmatrix} \cos\omega t & \sin\omega t \\ -\sin\omega t & \cos\omega t \end{bmatrix}\begin{bmatrix} v_{g\alpha} \\ v_{g\beta} \end{bmatrix} \tag{13}$$

By substituting Equation (11) into Equation (13), the voltage components in the *dq* frame can be rewritten as:

$$\begin{bmatrix} v_{gd} \\ v_{gq} \end{bmatrix} = \begin{bmatrix} \cos\omega t & \sin\omega t \\ -\sin\omega t & \cos\omega t \end{bmatrix}\begin{bmatrix} v_{i\alpha} - L\frac{di_\alpha}{dt} \\ v_{i\beta} - L\frac{di_\beta}{dt} \end{bmatrix} \tag{14}$$

To further simplify, Equation (15) expresses the relationship between the inverter voltages in the *dq* reference frame:

$$\begin{bmatrix} v_{gd} \\ v_{gq} \end{bmatrix} = \begin{bmatrix} v_{id} \\ v_{iq} \end{bmatrix} - L \begin{bmatrix} \cos \omega t & \sin \omega t \\ -\sin \omega t & \cos \omega t \end{bmatrix} \begin{bmatrix} \frac{di_\alpha}{dt} \\ \frac{di_\beta}{dt} \end{bmatrix} \quad (15)$$

Since the derivative terms in the $\alpha\beta$ frame can be rewritten as the time derivatives of the dq components plus an additional rotational term, the transformation matrix can be expressed as:

$$\begin{bmatrix} \cos \omega t & \sin \omega t \\ -\sin \omega t & \cos \omega t \end{bmatrix} \begin{bmatrix} \frac{di_\alpha}{dt} \\ \frac{di_\beta}{dt} \end{bmatrix} = \frac{d}{dt} \begin{bmatrix} i_d \\ i_q \end{bmatrix} + \omega \begin{bmatrix} -i_q \\ i_d \end{bmatrix} \quad (16)$$

Thus, the electrical dynamics of the inverter in the dq reference frame can be expressed in Equation (17), where the grid voltage components are related to the inverter control variables and inductive properties.

$$\begin{bmatrix} v_{gd} \\ v_{gq} \end{bmatrix} = \begin{bmatrix} v_{id} \\ v_{iq} \end{bmatrix} - L \frac{d}{dt} \begin{bmatrix} i_d \\ i_q \end{bmatrix} - \omega L \begin{bmatrix} -i_q \\ i_d \end{bmatrix} \quad (17)$$

Rearranging Equation (17), the final expression for the inverter control voltages in the dq frame is obtained in Equation (18). This form is useful in designing controllers for regulating the active and reactive power injection into the grid.

$$\begin{bmatrix} v_{id} \\ v_{iq} \end{bmatrix} = \begin{bmatrix} v_{gd} \\ v_{gq} \end{bmatrix} + L \frac{d}{dt} \begin{bmatrix} i_d \\ i_q \end{bmatrix} - \omega L \begin{bmatrix} -i_q \\ i_d \end{bmatrix} \quad (18)$$

This transformation and analysis are fundamental in synchronizing the inverter with the grid while ensuring efficient power flow control.

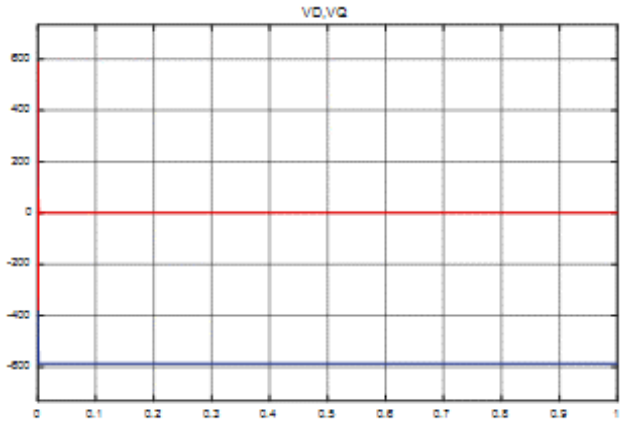

Figure 7: Relationship between V_d and V_q in GTI

Figure 7 illustrates that when $V_d = 0$ and $V_q \neq 0$, the GTI does not extract active power from the inverter to supply the grid. The value $V_q = -600$ VAR indicates the reactive power drawn by the inverter for voltage regulation and grid stability.

Hence, the synchronization equation can be derived as:

$$\frac{d}{dt} \begin{bmatrix} i_d \\ i_q \end{bmatrix} = \frac{1}{L} \begin{bmatrix} v_{id} - v_{gd} \\ v_{iq} - v_{gq} \end{bmatrix} - \omega \begin{bmatrix} -i_q \\ i_d \end{bmatrix} \quad (19)$$

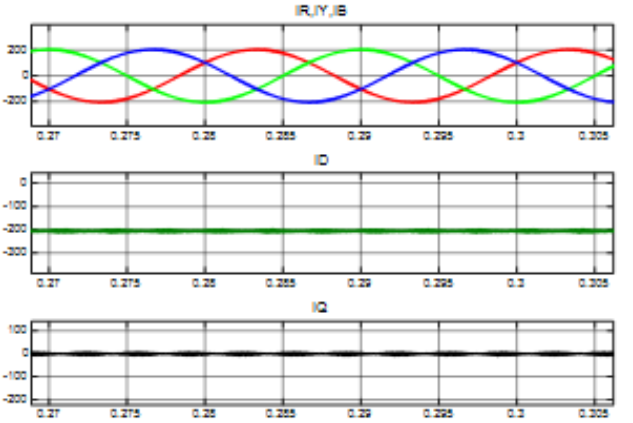

Figure 8: Relationship between I_{RYB}, I_d, and I_q

vi. Angle ωt or θ Generation in PLL Synchronization

As previously stated, injecting current from the photovoltaic power generation system into the grid requires that the phase and frequency be synchronized. Therefore, the inverter's output parameters require a `Phase Locked Loop (PLL)` to generate a reference current that controls the inverter current. This mechanism ensures proper reactive power delivery to the grid.

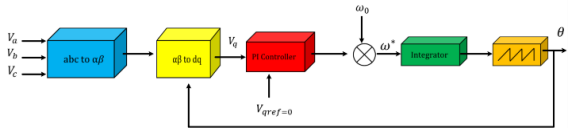

Figure 9: Generation of angle θ

Figure 9 illustrates the `PLL block` for phase detection and the generation of angle θ. The PLL produces a signal that is phase-shifted by 90° from the actual voltage. There are two methods to generate a PLL signal: open-loop control and closed-loop control. Open-loop control has weaknesses, including susceptibility to harmonic disturbances, which may result in incorrect phase angle estimation. The second method, closed-loop PLL, is employed to overcome these limitations.

Figure 10 shows the angle θ generation process in the PLL, beginning with the transformation from the *abc* reference frame to the $\alpha\beta$ reference frame. The

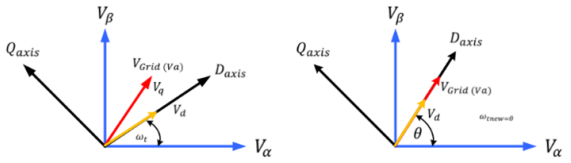

Figure 10: Vector relationship between V_d, V_q in the transformation of V_α, V_β

$\alpha\beta$ signals are then converted into the dq reference frame, where the axes are initially misaligned with the grid voltage. This results in nonzero values for V_d and V_q. The angle ωt is defined as the angle between the voltage vector and the α component.

To align V_d with the d-axis while ensuring $V_q = 0$, a modification process is carried out, leading to a newly computed ωt. This value is then used to generate both the active and reactive power components. The output of the PI control is fed into an integrator to determine θ, which is essential for constructing sinusoidal and cosinusoidal functions needed for active and reactive power generation.

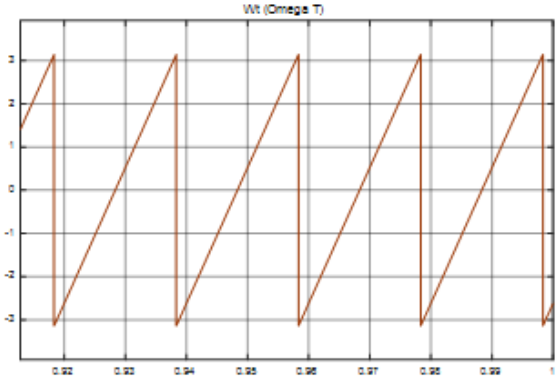

Figure 11: Generation of the omega-theta angle

Figure 11 presents the waveform of the theta angle produced by the PLL synchronizer. This waveform has a magnitude of 90°, which is used for generating sinusoidal and cosinusoidal components in active and reactive power calculations.

Figure 12 demonstrates that when $V_d = 0$ and $V_q \neq 0$, the GTI does not supply active power from the inverter to the grid. However, $V_q = -600$ VAR indicates that the inverter is supplying reactive power for voltage regulation and grid stability.

The PI controller is utilized to regulate i_d and i_q, allowing the inverter reference voltage to be expressed as:

$$\begin{bmatrix} v_{id}^* \\ v_{iq}^* \end{bmatrix} = \begin{bmatrix} v_{gd} \\ v_{gq} \end{bmatrix} + \begin{bmatrix} \left(k_p + \frac{k_i}{s}\right)(i_d^* - i_d) \\ \left(k_p + \frac{k_i}{s}\right)(i_q^* - i_q) \end{bmatrix} + \omega L \begin{bmatrix} -i_q \\ i_d \end{bmatrix} \tag{20}$$

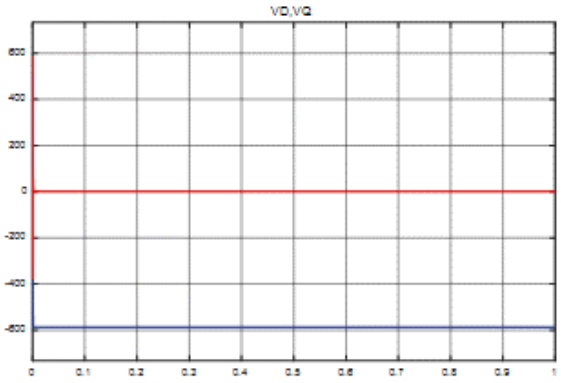

Figure 12: Relationship between V_d and V_q in GTI

The reference variables, denoted by the asterisk $(*)$, indicate that all computations are performed in the dq coordinate system. Within this reference frame, the active and reactive power of the inverter can be mathematically expressed. The active power P_{dq} is determined by the relationship between the direct and quadrature components of voltage and current, as given in Equation (21).

$$P_{dq} = \frac{3}{2}(V_d I_d + V_q I_q) \tag{21}$$

Similarly, the reactive power Q_{dq} is influenced by the interaction of the voltage and current components, as shown in Equation (22).

$$Q_{dq} = \frac{3}{2}(V_q I_d + V_d I_q) \tag{22}$$

These equations highlight the importance of proper voltage and current control in the dq reference frame to ensure efficient power delivery to the grid. Maintaining an accurate estimation of P_{dq} and Q_{dq} is crucial for optimizing inverter operation, reducing power losses, and enhancing overall system stability.

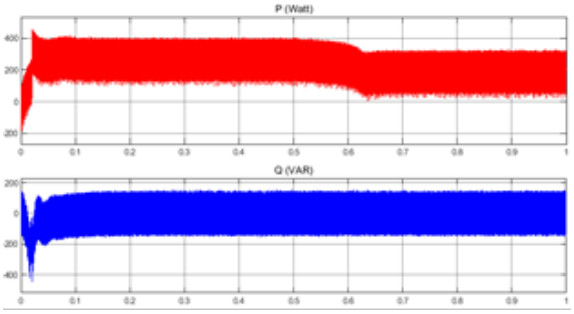

Figure 13: Active and reactive power values of GTI

Figure 13 illustrates the amount of active and reactive power delivered by the GTI to the grid, based on Equations (21) and (22). This power is supplied to the electrical network to compensate for increasing load demands.

The direct-axis (i_d^*) and quadrature-axis (i_q^*) currents play a crucial role in determining the active and reactive power flow in the dq reference frame. These currents are derived from the real and reactive power equations and are formulated to optimize power delivery to the grid.

The direct-axis current component, i_d^*, is responsible for regulating the active power injected into the grid. It is given by Equation (23), where it is expressed as a function of the direct and quadrature voltage components along with the real and reactive power components.

$$i_d^* = \frac{2}{3}\frac{(P_{dq}V_d - Q_{dq}V_q)}{(V_d^2 + V_q^2)} \tag{23}$$

Similarly, the quadrature-axis current component, i_q^*, determines the reactive power contribution of the inverter to the grid. It is formulated in Equation (24), showing its dependence on both active and reactive power components in relation to the direct and quadrature voltages.

$$i_q^* = \frac{2}{3}\frac{(P_{dq}V_q - Q_{dq}V_d)}{(V_d^2 + V_q^2)} \tag{24}$$

These equations are fundamental in grid-tied inverter control strategies, as they enable precise regulation of active and reactive power exchange. By accurately adjusting i_d^* and i_q^*, the inverter can enhance grid stability, improve power factor correction, and optimize energy efficiency.

vii. Analysis of Inverter Switch Trigger Pulses

The PWM triggering signal for the grid-tie inverter plays a crucial role in controlling the power switches during the DC-to-AC power conversion process while maintaining synchronization with the grid. PWM regulates the pulse width to control the AC voltage and frequency, ensuring that the inverter operates in phase with the electrical grid.

To generate the trigger signal for the inverter switches, a comparator-based approach is employed, utilizing a reference signal and a carrier signal. The reference signal ($V_{\text{ref}} = V_{abc}$) is a three-phase sinusoidal waveform with an amplitude of 0.85 Vpp at 50 Hz. Meanwhile, the carrier signal (V_{carrier}) is a triangular waveform with an amplitude of 1 Vpp and a frequency of 5 kHz.

Both signals are compared using a comparator circuit, which generates a series of pulses with adjustable pulse width at the output. The switching logic follows these rules: - If the carrier signal is higher than the reference signal, the comparator output is high. - If the carrier signal is lower than the reference signal, the comparator output is low.

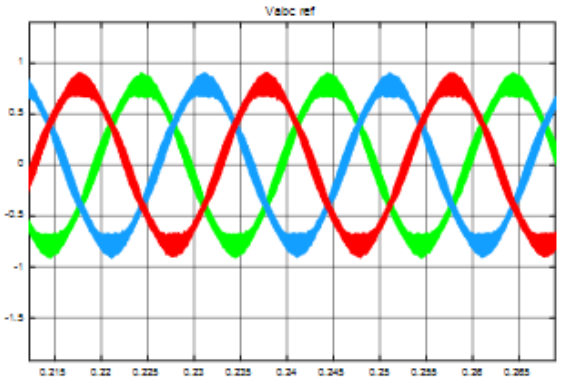

Figure 14: Reference signal waveform V_{abc}

Figure 14 illustrates the reference voltage waveform, which consists of three sinusoidal signals phase-shifted by 120°.

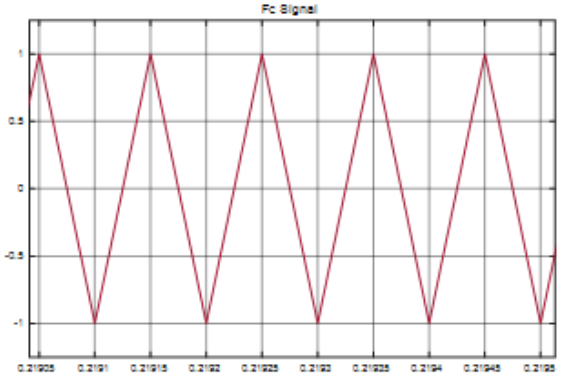

Figure 15: Triangular carrier signal

Figure 15 represents the carrier signal, which is a triangular waveform with an amplitude of 1 Vpp and a frequency of 5 kHz.

Figure 16 displays the generation of PWM pulses, where (a) illustrates the comparator-based PWM pulse generation process, and (b) shows the resulting PWM pulses.

Figure 17 presents the Total Harmonic Distortion (THD) index of the grid voltage, measured at 2.47%. Since this THD level is below the 5% threshold specified by the IEEE 519 standard, it is considered acceptable for a power system.

IV. Conclusion

The solar panel module generates a DC voltage of 125 V, which is increased to 700 V using a Boost converter with a maximum short-circuit current of 6.14 A. These two parameters are used to calculate the power (P) required to determine the active and reactive power components. To inject active and reactive power from the grid-tie inverter (GTI) into the grid,

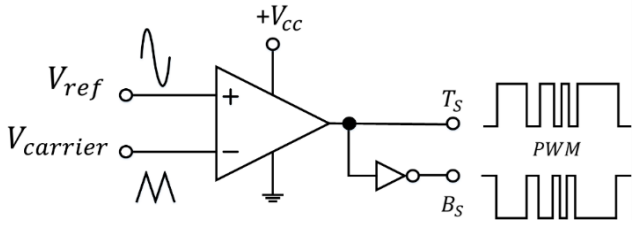

(a) PWM pulse generation using a comparator

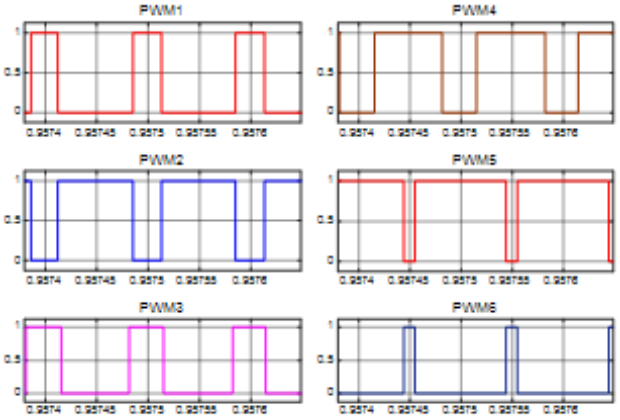

(b) Generated PWM trigger pulses

Figure 16: PWM pulse generation process

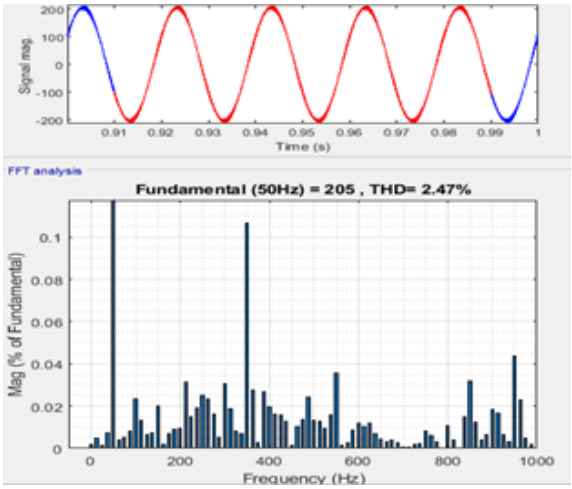

Figure 17: Total Harmonic Distortion (THD) index of GTI voltage

it must have the same voltage and phase difference, requiring a phase detector using a phase-locked loop (PLL). This is achieved through current and voltage sensor measurements and mathematical calculations that produce a phase angle of 90°. This phase angle is used to determine sine and cosine functions, where these trigonometric functions form the active and reactive power components generated by the inverter. The inverter switch requires a trigger pulse to operate and transfer power to the grid. The switching pulse is a PWM pulse obtained from a control process to match the power grid requirements through PI control. The additional power supplied by the inverter to the grid produces a sinusoidal grid voltage waveform with a total harmonic distortion (THD) value of 2.47%. This THD value indicates a low harmonic content, which is still tolerable and can be consumed by electrical system loads.

Acknowledgment

The authors express their gratitude to the Rector of Universitas Gunadarma for the support that enabled this research to be completed. Appreciation is also extended to colleagues in the Electrical Engineering Department for their valuable suggestions and motivation, which contributed to the successful completion of this research report.

References

[1] S. Jenderal and D. E. Nasional, "Outlook," 2023.

[2] P. Harahap, M. Adam, and B. Oktrialdi, "Optimasi kapasitas rooftop pv off grid energi surya berakselerasi di tengah pandemi covid-19 untuk diimplemtasikan pada rumah tinggal," vol. 5, no. 1, pp. 31–38, 2019.

[3] D. Hameed, S. Hamayoon, A. A. Malik, and O. A. Ansari, "Solar grid-tied inverter, with battery back-up, for efficient solar energy harvesting," pp. 95–99, 2016.

[4] S. Saodah and S. R. I. Utami, "Perancangan sistem grid tie inverter pada pembangkit listrik tenaga surya," vol. 7, no. 2, pp. 339–350, 2019.

[5] P. Dan, S. O. Photovoltaic, and M. Simulink, "Dengan grid-tied inverter menggunakan," vol. 6, no. 2, pp. 75–86, 2023.

[6] T. R. Tangga, "Pembangkit listrik tenaga surya (plts) sebagai solusi energi terbarukan rumah tangga," vol. 6, no. 2, pp. 136–142, 2022.

[7] M. Wahyu, A. Fauzi, M. N. Hidayat, and W. Anistia, "Analisis keandalan sistem grid tied inverter (gti) pada on-grid solar pv 9 x 80 wp," pp. 29–35.

[8] G. Patrianaya, M. Wirsuyana, R. S. Hartati, and I. B. Gede, "Metode maximum power point tracking pada panel surya: Sebuah tinjauan literatur," pp. 211–224.

[9] C. A. Belhadj, "Proposed simulator for testing mppt techniques for photovoltaic systems," 2021. [Online]. Available: https://doi.org/10.1109/IREC48820.2020.9310420

[10] A. Saleh, W. Hadi, and M. C. Anwar, "Desain kontrol maximum power point traker (mppt) menggunakan incremental conductance (inc) pada dc/dc tipe sepic," pp. 1–2, 2017.

[11] M. A. Islam, A. Merabet, R. Beguenane, H. Ibrahim, and H. Ahmed, "Simulation based study of maximum power point tracking and frequency regulation for stand-alone solar photovoltaic systems," 2014.

[12] Y. Zhu, M. K. Kim, and H. Wen, "Simulation and Analysis of Perturbation and Observation-Based Self-Adaptable Step Size Maximum Power Point Tracking Strategy with Low Power Loss for Photovoltaics," *Energies*, vol. 12, no. 1, p. 92, dec 28 2018. [Online]. Available: http://dx.doi.org/10.3390/EN12010092

[13] N. Li, C. Zhang, D. Wei, M. Liu, and Y. Zhang, "A boost converterbased MPPT steadystate oscillationfree fast tracking control strategy for photovoltaic power systems," *IET Power Electronics*, vol. 16, no. 3, pp. 483–497, sep 26 2022. [Online]. Available: http://dx.doi.org/10.1049/pel2.12400

[14] K. Javed, H. Ashfaq, and R. Singh, "An improved MPPT algorithm to minimize transient and steady state oscillation conditions for small SPV systems," *International Journal of Renewable Energy Development*, vol. 7, no. 3, pp. 191–197, dec 15 2018. [Online]. Available: http://dx.doi.org/10.14710/IJRED.7.3.191-197

[15] C.-C. Hua and Y.-J. Zhan, "A Hybrid Maximum Power Point Tracking Method without Oscillations in Steady-State for Photovoltaic Energy Systems," *Energies*, vol. 14, no. 18, p. 5590, sep 7 2021. [Online]. Available: http://dx.doi.org/10.3390/en14185590

[16] J. Ahmed and Z. Salam, "A Modified P&O Maximum Power Point Tracking Method With Reduced Steady-State Oscillation and Improved Tracking Efficiency," *IEEE Transactions on Sustainable Energy*, vol. 7, no. 4, pp. 1506–1515, 10 2016. [Online]. Available: http://dx.doi.org/10.1109/TSTE.2016.2568043

[17] S. Abuzed, M. Foster, and D. Stone, "Variable PWM step-size for modified Hill climbing MPPT PV converter," in *7th IET International Conference on Power Electronics, Machines and Drives (PEMD 2014)*. Institution of Engineering and Technology, 2014, pp. 4.5.05–4.5.05. [Online]. Available: http://dx.doi.org/10.1049/CP.2014.0489

[18] A. Saberi, M. Niroomand, and B. M. Dehkordi, "An Improved P&O Based MPPT for PV Systems with Reduced Steady-State Oscillation," *International Journal of Energy Research*, vol. 2023, pp. 1–15, jul 22 2023. [Online]. Available: http://dx.doi.org/10.1155/2023/4694583

[19] M. M. A. Awan, "Technical Review of MPPT Algorithms for Solar Photovoltaic System: Swot Analysis of MPPT Algorithms," *Sir Syed University Research Journal of Engineering & Technology*, vol. 12, no. 1, pp. 98–106, jun 30 2022. [Online]. Available: http://dx.doi.org/10.33317/ssurj.433

[20] T. E. Industri, P. Elektronika, and N. Surabaya, "Perancangan mppt modified incremental conductance menggunakan interleaved boost converter untuk reduksi osilasi," vol. 10, no. 1, pp. 76–89, 2022.

[21] E. Science, "Effectiveness of solar panel positioning and grid tie inverter (gti) in generating solar energy in indonesian houses." [Online]. Available: https://doi.org/10.1088/1755-1315/1016/1/012050

[22] A. Hafid, P. Studi, T. Elektro, U. Muhammadiyah, G. T. Inverter, and S. Matlab, "Simulasi pusat tenaga listrik (plts) on grid pada jaringan tegangan rendah menggunakan simulink matlab," vol. 6, no. 1, pp. 32–37, 2023.

[23] K. Sistem, K. Plts, and O. Di, "No title."

[24] J. Siwalankerto, "Analisa daya pada pemanfaatan panel surya," vol. 6, no. 2, pp. 106–112, 2024.

[25] S. Purnomo, Y. Z. Arief, A. Jaenul, S. Wilyanti, and I. Artikel, "Analisis pengaruh cuaca terhadap efisiensi panel surya grid tie menggunakan konfigurasi micro inverter dan string inverter terhadap energi yang dihasilkan," vol. 12, no. 2, pp. 100–110, 2023. [Online]. Available: https://doi.org/10.35508/jme.v12i2.12648

[26] R. A. Diantari, H. Suyanto, and S. Hidayat, "Analysis inverter of plts on grid," in *2023 7th Int. Conf. Electron. Mater. Eng. Nano-Technology*, 2023, pp. 1–6. [Online]. Available: https://doi.org/10.1109/IEMENTech60402.2023.10423517

[27] M. G. Muftah, M. Salem, Y. M. Buswig, K. B. Hamad, D. N. Luta, and M. Kamarol, "A grid-tied pv-fuel cell multilevel inverter under pq open-loop control scheme," pp. 1–17, 2022. [Online]. Available: https://doi.org/10.3389/fenrg.2022.968371

[28] T. P. W. M. Inverter, Y. Pratomo, D. F. Marmora, and P. A. Dahono, "Design and analysis of three-phase," pp. 1–5.

[29] S. Das and E. Hossain, "Fixed point implementation of grid tied inverter in digital signal processing controller," 2020. [Online]. Available: https://doi.org/10.1109/ACCESS.2020.2993985